PERGAMON International Journal of Mechanical Sciences 41 (1999) 235–248

International Journal of MECHANICAL SCIENCES

Pressure response and droplet ejection of a piezoelectric inkjet printhead

Ping-Hei Chen[a,*], Hsin-Yah Peng[a], Hsin-Yi Liu[a], S.-L. Chang[a], T.-I. Wu[a], Chiang-Ho Cheng[b]

[a] *Department of Mechanical Engineering, National Taiwan University No.1, Sec. 4, Roosevelt Rd., Taipei 10617, Taiwan, ROC*
[b] *Dialer and Business Electronics Co. Ltd., No.29-1, Tzu Chiang Street, Tu-Cheng, Taipei, Taiwan*

Received 5 August 1997; received in revised form 8 May 1998

Abstract

The present study aims to investigate the pressure rise in the ink flow channel and the ink droplet formation process of a piezoelectric printhead after an electrical pulse is applied to the printhead. The ink flow channel is modeled as a straight circular pipe followed by a convergent nozzle. Both numerical analysis and experimental observations are performed in this study. In the numerical analysis, a characteristic method is used to solve the one-dimensional wave equation to obtain the transient pressure and velocity variations in the flow channel of the printhead. In this analysis, the channel is assumed to have a non-uniform cross section. In addition, a flow visualization system was set up to observe the ink droplet injection process. After the piezoelectric material is driven by the input electric pulse, the ink droplet images are immediately captured by a charge-couple device (CCD) camera converted to a digital image via a frame grabber, and stored in a computer. The results obtained from the experimental observations are also compared with the numerical prediction. The effects of electric pulse shape and voltage on the ink injection length and the ejected droplet weight are also presented.

Keywords: piezoelectric inkjet printhead; flow visualization; wave equation

Nomenclature

A	cross-sectional area of the ink flow channel
a	wave speed in the ink flow channel
D	equivalent hydraulic diameter of the ink flow channel
D_1	diameter of the nozzle inlet, as shown in Fig. 2
D_2	diameter of the nozzle exit, as shown in Fig. 2
E	operating voltage of the electric pulse

* Corresponding author. Tel.: 00886 2 2363 0231; fax: 00886 2 2363 1755; e-mail: phchen@ ccms.ntu.edu.tw.

0020-7403/99/$ – see front matter
PII: S0020-7403(98)00058-7

f Darcy friction factor
g gravitational acceleration
L total length of the ink channel
L_1 length of the simplified ink flow channel with constant cross section, as shown in Fig. 2
p ink pressure
p_0 initial pressure in the ink
Re Reynolds number, $\mathrm{Re} = \rho u D/\mu$
u ink velocity
T1 charging time interval of electric pulse, as shown in Fig. 4
T2 discharging time interval of electric pulse, as shown in Fig. 4
T3 rest time interval of electric pulse, as shown in Fig. 4
t elapsed time from the application of the electric pulse to the piezoelectric transducer
x streamwise coordinate
W averaged weight of a single ink droplet

Greek letters
α angle between the centerline of the ink channel and the horizontal plane
μ ink viscosity
θ angle between the centerline of the flow channel and the channel wall
ρ ink density

Subscripts
i ith node along the x coordinate in the computational mesh
j jth time increment in the computational mesh

1. Introduction

In recent years, the sales of the drop-on-demand inkjet printhead have dramatically grown because of its low price in both monochromatic and color printing. There are two popular types of inkjet printheads in the commercial market, namely the thermal bubble inkjet and piezoelectric inkjet printheads. Whel [1] and Mills [2] have both provided excellent reviews of the advantages and the fundamental limitations of drop-on-demand ink-jet printing. There are three types of piezoelectric printheads in the market, namely the piezo-tube, the piezo-diaphragm, and the piezo-lamella. The print quality and resolution of an inkjet printhead is directly affected by the formation of satellite droplets, the ink droplet size, and the droplet injection frequency. Without detailed knowledge of the pressure response and velocity variation in the ink flow channel, optimal droplet ejection and therefore optimal printing quality cannot be assured.

This study investigates the droplet ejection process of a piezoeletric inkjet printhead. For the thermal inkjet printhead, both the flow visualization experiment and the numerical analysis on the droplet ejection process were presented by Chen *et al.* [3]. In the study of Beasley [4], the ink in the flow channel is assumed to be incompressible and a one-dimensional hydraulic equation of motion for the piezo-tube inkjet channel was derived using Newton's second law. Effects of flow channel non-uniform cross section on the ink flow velocity are captured by the effective inertia and viscous lengths defined in his study. Bogy and Talke [5], on the other hand, solved the one-dimensional

wave equation for the ink flow in a constant cross-section piezo-tube inkjet channel. In their theoretical predictions, the nozzle exit was assumed to be closed. The same incompressible one-dimensional hydraulic equation as the one in Beasley [4] was also used to describe the ink flow in the nozzle connected to the piezoelectric tube in the work of Shield *et al.* [6]. Two separate equations of motion were used by Shield *et al.* [6]. These are called the hybrid model in this paper. The formation process for nozzle-ejected droplets was modeled using a finite-difference scheme to solve the Navier–Stokes equation in cylindrical coordinates. There is strong agreement between numerical predictions of droplet deformation and experimental observations. The shape evolution of ejected droplets was also reported by Fromm [7] with known square wave pressure histories applied to the inlet of the ink nozzle. Navier–Stokes equations in axisymmetric coordinates were solved using a finite-difference scheme in a Lagrangian computational mesh. Berchtold [8] also used the hybrid model to describe the ink flow motion in a printhead with the bilaminar piezoelectric transducer. A finite-element method was used to determine the effects of the electric pulse shape and the diameter of the round nozzle on the average velocity of the ejected droplet. It was found that the velocity can range from 0 to 5.0 $m\,s^{-1}$ depending on the applied electric pulse and the nozzle diameter.

In this paper, the object is to investigate the piezo-diaphragm printhead by employing both numerical simulation and experimental observations. Most prior studies evaluated the transient pressure and flow velocity variations in the flow channel of the piezo-tube printhead using the hybrid model. In the present ink flow channel, the one-dimensional wave equation was numerically solved for the ink flow velocity from the surface of the piezo-diaphragm transducer (or displacer) to the exit of the convergent ink nozzle. In addition, an inexpensive flow visualization system was set up to observe the injection process of the ink droplet. The flow visualization results are also compared with the numerical predictions. The effects of electrical pulse shape and voltage in the piezo-diaphragm displacer on the ejected droplet length and the droplet weight are also examined.

2. Theoretical model and numerical analysis

A single ink ejection system of a commercial piezo-diaphragm printhead is shown in Fig. 1. From top to bottom, this ink ejection system consists of a protection layer, a nozzle plate, a spacer, a pressure chamber (or an ink flow channel), a diaphragm, and a piezoelectric transducer. The convergent nozzle has a circular cross section with an inlet-to-outlet area ratio of 4. The inlet diameter, outlet diameter, and height are 40, 80, and 80 μm, respectively. The height of the pressure chamber from the diaphragm to the nozzle plate is 220 μm. Above the piezoelectric transducer is the nickel piezo-diaphragm vibrating displacer. Note that the portion of nickel diaphragm under the spacer is fixed. The nickel diaphragm has a flexible thin region, with a thickness of 2 μm. The piezoelectric transducer has a rectangular cross section of 500 mm × 50 mm. Above the transducer, the moving portion of the nickel diaphragm has a cross-sectional area of 0.21 mm^2. The ink, of which 86.5% is water, has physical properties similar to water, and the dynamic viscosity is 1.28 cp. Although the flow motion in the pressure chamber for a commercial piezo-diaphragm printhead is three-dimensional, a one-dimensional approach has been adopted for this study. Thus, a simplified circular pipe followed by a convergent nozzle is employed to simulate the ink pressure chamber for the commercial printhead, as illustrated in Fig. 2. Under the assumption that the ink in the pressure

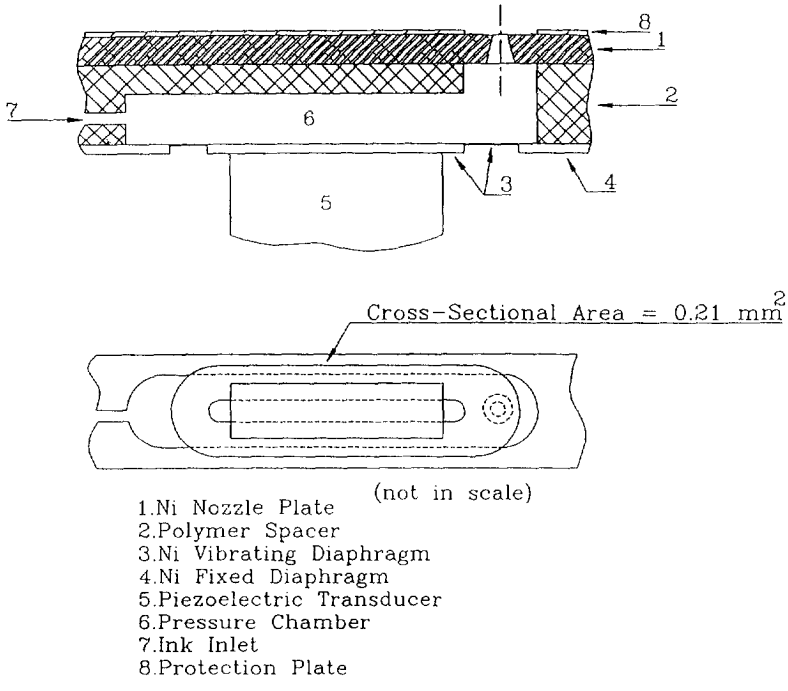

Fig. 1. Schematic view of a commercial piezo-diaphragm printhead (not to scale).

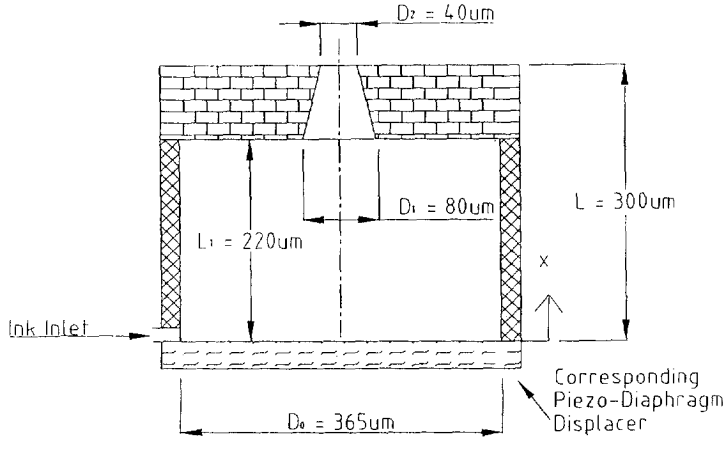

Fig. 2. A simplified circular pipe representation of the commercial piezo-diaphragm printhead (not to scale).

chamber is equally divided between the nozzle and the ink reservoir after the forward motion of the piezo-diaphragm displacer, the cross-sectional area of the circular pipe is taken to be equal to half the cross-sectional area of the moving portion of the nickel diaphragm. Further, the ink flow motion in the simplified channel is described by the one-dimensional wave equation. The

one-dimensional continuity and momentum equations for the ink flow motion are expressed as

$$\frac{D}{Dt}(\rho A\, dx) = 0, \tag{1}$$

$$\frac{D}{Dt}(\rho Au\, dx) = \sum F, \tag{2}$$

where ρ is the ink density, assumed constant for a typical working pressure less than 0.5 MPa in the piezo-diaphragm printhead and F is the force exerted on the ink.

With an impulse movement of the piezo-diaphragm displacer, the resultant transient flow phenomenon in the ink flow channel is similar to the water-hammer phenomenon in a piping system, and the continuity and momentum equations can be further derived into the following forms

$$\frac{1}{\rho a^2}\frac{Dp}{Dt} + \frac{u}{A}\sigma(x) + \frac{\partial u}{\partial x} = 0, \tag{3}$$

$$\rho\frac{\partial u}{\partial t} + \rho u\frac{\partial u}{\partial x} = -\frac{\partial p}{\partial x} - \rho g\sin\alpha - \frac{fu|u|\cos\theta}{2D\,dx}, \tag{4}$$

where a denotes the wave speed in the ink fluid, $\sigma(x) = \partial A/\partial x$ is the gradient of the cross-sectional area, α denotes the angle between the centerline of the ink pipe and the horizontal plane, and θ represents the angle between the centerline of the pipe and the pipe wall. Since the ink channel wall is mainly made of silicon, which has a high elastic modulus, the wave speed in the ink is assumed to have a constant value.

When Eqs. (3) and (4) are solved for both velocity and pressure using the characteristic method, the corresponding compatibility equations are

$$\frac{1}{\rho a}\frac{dp}{dt} + \frac{du}{dt} + g\sin\alpha + \frac{fu|u|\cos\theta}{2Ddx} + \frac{ua}{A}\sigma(x) = 0, \tag{5}$$

$$\frac{dx}{dt} = u + a \quad \text{on } C^+, \tag{6}$$

$$\frac{1}{\rho a}\frac{dp}{dt} - \frac{du}{dt} - g\sin\alpha - \frac{fu|u|\cos\theta}{2D\,dx} + \frac{ua}{A}\sigma(x) = 0, \tag{7}$$

$$\frac{dx}{dt} = u - a \quad \text{on } C^-, \tag{8}$$

where f denotes the Darcy friction factor. For laminar flow, the Darcy friction factor is given as $f = 64/\mathrm{Re}$. As shown in Fig. 3, C^+ and C^-, defined in Eqs. (6) and (8), denote characteristic lines in the x-t plane. For $dx/dt \neq \pm a$, neither characteristic line which intersects at the $(i, j+1)$ node passes through the mesh nodes on the jth time increment. It is expected that both characteristic lines are nonlinear because u is a function of x and t.

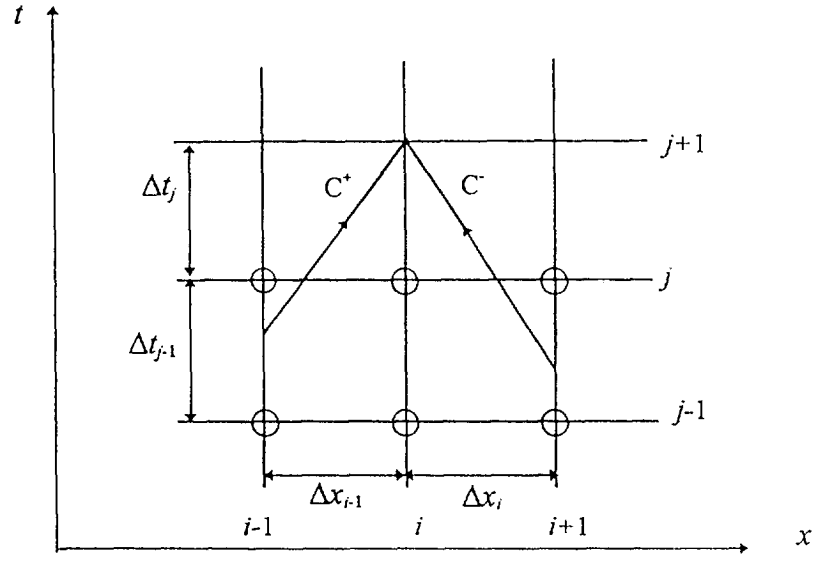

Fig. 3. The discretization used for the method of characteristic calculation in the device chamber.

The initial and boundary conditions for Eqs. (5)–(8) are given by

$$\text{IC:}\quad \begin{aligned} u(x,0) &= 0, \\ p(x,0) &= p_0, \end{aligned} \tag{9}$$

$$\text{BC:}\quad \begin{aligned} u(0,t) &= f(t), \\ p(L,t) &= p_0, \end{aligned} \tag{10}$$

where p_0 denotes the initial ink pressure and $f(t)$ is the time-dependent averaged moving velocity of the piezo-diaphragm displacer after an electric pulse is applied to the piezoelectric material of the test printhead. The pressure loss caused by the sudden contraction occurring at the intersection of the circular pipe and the nozzle is neglected.

The function $f(t)$ describing the motion of the piezo-diaphragm displacer under the applied electric pulse, is determined using the ANSYS 5.0A finite-element software package. Fig. 4 shows a typical triangular electrical pulse applied to the piezoelectric transducer with three time intervals T1, T2 and T3. The T1, T2, and T3 time intervals are called the charging, discharging, and resting time intervals, respectively. The ejection frequency of the ink droplets from the printhead is equal to 1/(T1 + T2 + T3). In the first time interval T1, the piezoelectric piece withdraws as the operating voltage linearly drops from zero to + 25 V. The piezoelectric piece then moves towards the nozzle while the operating voltage of the electric pulse drops from +25 V to zero. While the electric voltage is kept at zero volts for a period of T3, the piezo-diaphragm displacer undergoes a damped oscillation before it stops completely. The piezo-diaphragm displacer is triggered again by the electric pulse at the end of period T3. A typical velocity response of the piezo-diaphragm displacer is shown in Fig. 5 for a triangular electric pulse with T1 = 90 μs, T2 = 9 μs and T3 = 55 μs at E = 25 V.

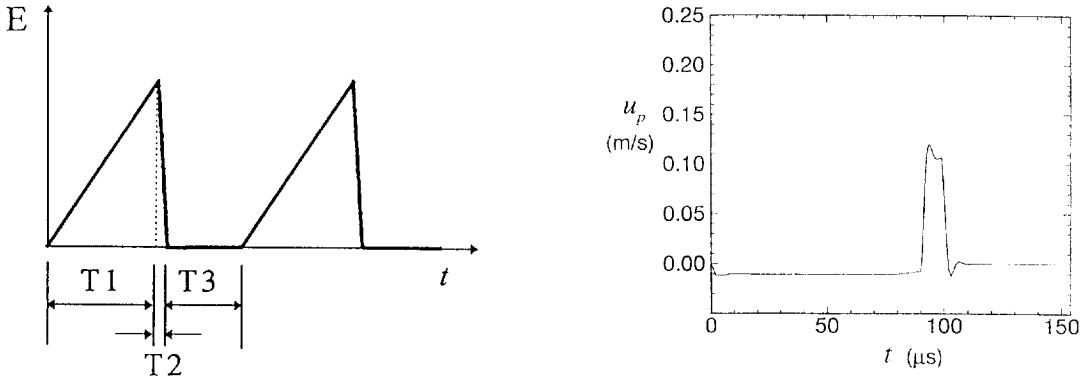

Fig. 4. A typical triangular electrical pulse.

Fig. 5. Velocity response of the piezo-diaphragm displacer at T1 = 90 μs, T2 = 9 μs, T3 = 55 μs, and E = 25 V. (generated using ANSYS 5.0A).

A forward-time centered-space finite-difference method was used for solving Eqs. (5)–(10). Thus, the numerical scheme has a first-order accuracy in time and a second-order accuracy in space. To obtain convergent solutions, the Courant–Friedrichs–Lewy stability criterion, $a(\Delta t/\Delta x) \leqslant 1$, should be satisfied. In this study, the time increment is obtained by

$$\Delta t = \frac{\Delta x}{a} \tag{11}$$

A numerical test was performed on the predicted solutions for T1 = 90 μs, T2 = 9 μs, T3 = 55 μs, and $E = 25$ V. The numerical results were obtained for mesh numbers varying from 100 to 500 nodes. The maximum variation in pressure at the nozzle inlet is less than 0.6% as the mesh number increases from 300 to 400. Thus, a 300-node mesh was used in all numerical tests.

3. Experimental observations

An experimental system was set up to observe the droplet ejection process at different time instants and to measure the mass of the ink droplets. The experimental apparatus consists of a commercially available piezo-diaphragm printhead, an electronic system, and an image capturing system (Fig. 6). As shown in Fig. 1, the test commercial printhead has an ink reservoir, a nickel nozzle plate, a polymer spacer, and a piezo-diaphragm displacer. The vibrating diaphragm is attached to the piezoelectric transducer which is driven by triangular pulses at a fixed frequency ranging from 3 to 8 kHz. This is significantly faster than the 1 kHz ejection rate for a typical thermal bubble inkjet printhead. Using a strobe light, it is possible to view the formation of the droplets with a charge-coupled device (CCD) camera. The electronic system consists of a customer-made controller with a liquid crystal display (LCD), a power supply, a Hitachi VC-6025 digital oscilloscope, and a light emitting diode (LED) stroboscope. The controller can convert

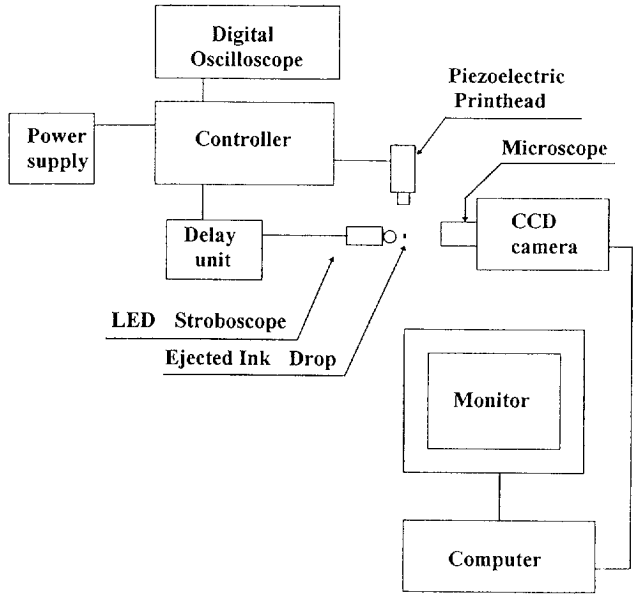

Fig. 6. Schematic view of the optical system for ink ejection visualization.

a DC voltage from the power supplier into a triangular wave, as shown in Fig. 4. All three time intervals T1, T2, and T3 and the operating voltage of the triangular pulse can be individually varied. The electric pulse accuracy is continuously monitored by the digital oscilloscope. All of the parameters can be read from the LCD panel of the controller. In addition, the synchronized lighting for the LED strobe is controlled by the controller. The droplet ejection process beyond the ink nozzle can be visualized at distinct time instants by modifying the phase shift between the electric pulse and the strobe light pulse.

The image capturing system includes a 10 × microscope, a Model IK-536 CCD camera made by Toshiba, a three-axis precision table, an IBM-compatible 486 personal computer with a monochrome frame grabber. The printhead was installed on the top of the three-axis table and the nozzle exit was oriented downwards. After the piezo-diaphragm displacer is driven by the input electric pulse, the ink travel distance is observed through a 10 × microscope using a synchronized stroboscope light emitted from the LED. The ejected ink image captured by the CCD camera is then digitized by the frame grabber, stored as a file in the computer, and is shown on the computer monitor. The ejected ink length can be directly measured from the ink image shown on the monitor screen. Since the smallest step that can be moved by the precision table is 0.005 mm, with the image magnification by the microscope and the monitor, the estimated uncertainty in the measured travel distance is $\pm$ 6.0 μm (20/1 odds).

The ejected ink droplets are caught in a plastic container. After ten million ink droplets are ejected, the total weight is measured by an electronic scale made by Presica. This electronic scale has a resolution of 0.1 mg. Accordingly, based on a 95% confidence level, the operating voltage, the time intervals T1, T2, and T3, and the ejected number of droplets were measured from the electrical pulse shown on the digital oscilloscope within a range of $\pm$ 3%. Thus, estimated by an uncertainty analysis [9], the uncertainty of the averaged weight of a single ink droplet is within $\pm$ 0.02 ng.

Flow visualization measurements were conducted at different combinations of operating voltage and T1, T2, and T3 time intervals. However, no significant effects of T1 and T3 on the ejected ink length and weight were observed in the measured results. Therefore, the results over a range of T2 and operating voltage values for constant T1 = 90 μs and T3 = 55 μs. Numerical predictions are presented for T2 values ranging from 5 to 15 μs at $E = 25$ V, and for E values ranging from 15 to 25 V at T2 = 9 μs. Comparison is made between the predicted and measured averaged weight of a single ink droplet.

4. Results and discussion

The image results are presented as a series of photographs taken directly from the monitor by the use of a Nikon F1 camera. Fig. 7 shows the ink ejection process at eight time instants for $E = 25$ V, T1 = 90 μs, T2 = 9 μs, and T3 = 55 μs. Over all combinations of operating voltages and time intervals, the ejection process of the ink droplet is similar to the one shown in Fig. 7. As time progresses after the electric pulse is applied to the piezoelectric transducer, the ink ejected out of the nozzle gradually changes its shape from a cylindrical column to an eyedrop-like shape at $t = 107$ μs (Fig. 7a). This shape is formed because the ejected ink has a higher velocity at the drop tip than that at the nozzle exit. This probably results from the fact that less frictional force is exerted on the droplet by the surrounding air than by the solid nozzle. In Fig. 7d ($t = 140$ μs), the breakup of the ejected ink can be observed. In other words, the ejected ink separates from the nozzle exit. At $t = 140$ μs, the tip of the ink droplet is 398 μm away from the nozzle exit. The single round droplet is not formed until $t = 151$ μs, as shown in Fig. 7f. Fig. 7f also clearly shows that a satellite droplet appears after the formation of the main ink droplet at $t = 151$ μs. This formation of the satellite droplet may seriously affect the printing quality. The satellite droplet will not reach the paper surface at the designated spot like the main droplet because the printhead continuously moves during the ejection process. For all electric pulses tested in this study, a satellite droplet was always formed. Therefore, it remains a challenge for researchers to find a feasible way to eliminate the formation of satellite droplets.

The effect of the discharging time interval T2 on the transient variation of droplet ejection length is illustrated in Fig. 8. The open circle symbols in Fig. 8 denote the time at which the ejected ink separates from the nozzle exit. Since the displacement of the piezoelectric transducer is only affected by the operating voltage of the electric pulse, the transient velocity of piezo-diaphragm displacer increases with a reduction in the discharging time interval. Consequently, a greater pressure rise in the pressure chamber is expected for the test with a smaller discharge time. As a result, more ink is driven out of the pressure chamber when a smaller discharge time interval is used. As seen in the measured results in Fig. 8, the ejected ink length increases with a decrease in T2. The growth of the ejected ink length is almost linear. This indicates that the drag resulting from the surrounding air on the ejected ink is rather small. However, the ejected ink velocity becomes too fast for the ink droplet to make a smooth contact on the paper surface if the value of T2 is less than 2 μs.

The transient ejected droplet lengths for the three operating voltages of 15, 20, and 25 V are shown in Fig. 9 for T1 = 90 μs, T2 = 9 μs, and T3 = 55 μs. An increase in the operating voltage results in a greater displacement of the vibrating piezo-diaphragm displacer. For the same

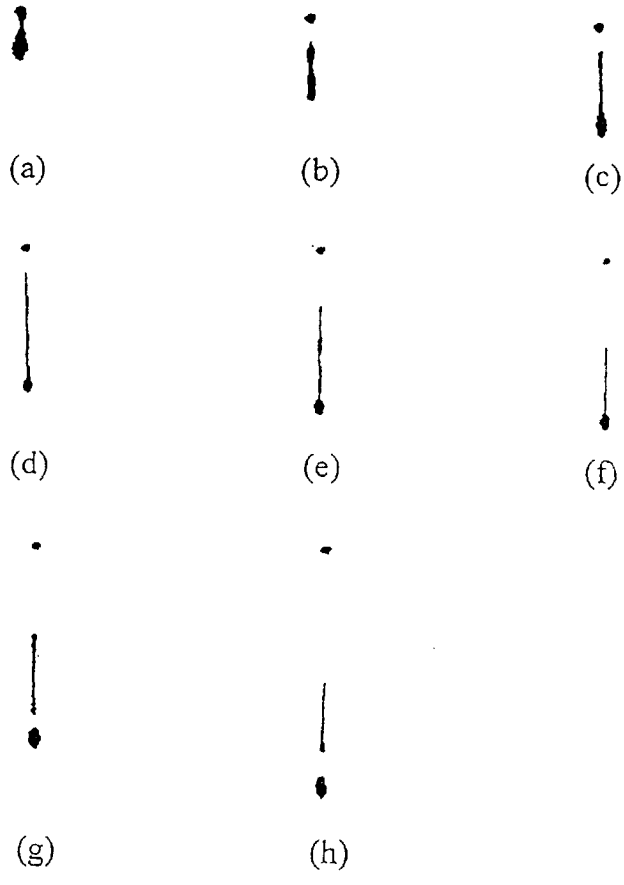

Fig. 7. Time elapsed ejected ink images at T1 = 90 μs, T2 = 9 μs, T3 = 55 μs, and E = 25 V: (a) t = 107 μs, L_d = 135 μm; (b) t = 120 μs, L_d = 231 μm; (c) t = 130 μs, L_d = 320 μm; (d) t = 140 μs, L_d = 398 μm; (e) t = 148 μs, L_d = 458 μm; (f) t = 151 μs, L_d = 470 μm; (g) t = 160 μs, L_d = 553 μm; (h) t = 175 μs, L_d = 673 μm.

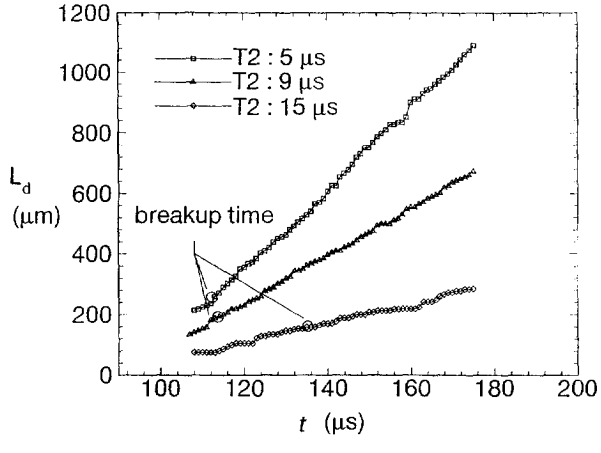

Fig. 8. Transient variation of the droplet ejection length for T1 = 90 μs, T3 = 55 μs, and E = 25 V at various T2 values.

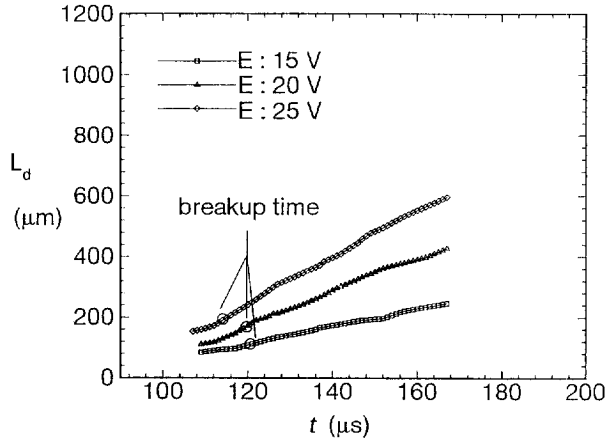

Fig. 9. Transient variation of the droplet ejection length for T1 = 90 μs, T2 = 9 μs, and T3 = 55 μs at various operating voltages.

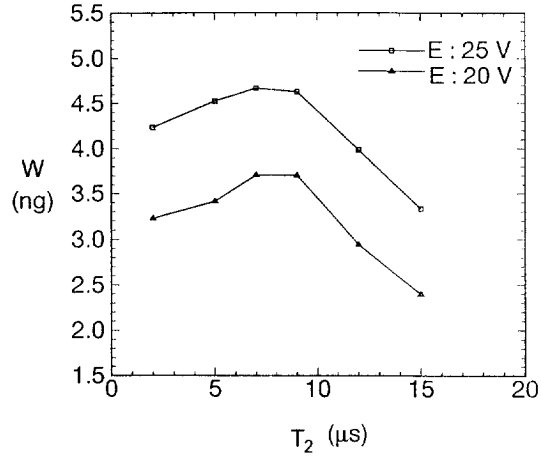

Fig. 10. Weight of a single ink droplet for T1 = 90 μs and T3 = 55 μs at various T2 values and operating voltages.

discharging time, the displacer is expected to have a higher velocity with a higher operating voltage. In Fig. 9, the ejected droplet length increases approximately linearly with the operating voltage. In addition, there was no appearance of satellite droplets for T1 = 90 μs, T2 = 9 μs, T3 = 55 μs, and $E = 15$ V in the flow visualization pictures that are not shown here. The ejected ink droplet has the same column shape as the one described in Hosono *et al.* [10].

The effect of discharging time T2 and operating voltage on the weight of a single ink droplet are shown in Fig. 10. A similar trend can be observed between the ejected ink droplet weight and discharge time at both $E = 20$ V and $E = 25$ V. With a greater operating voltage, the ejected ink droplet weight is higher because of the greater pressure rise in the pressure chamber. Regardless of the variation in the discharge time, the weight ratio of the ejected ink droplet between the two

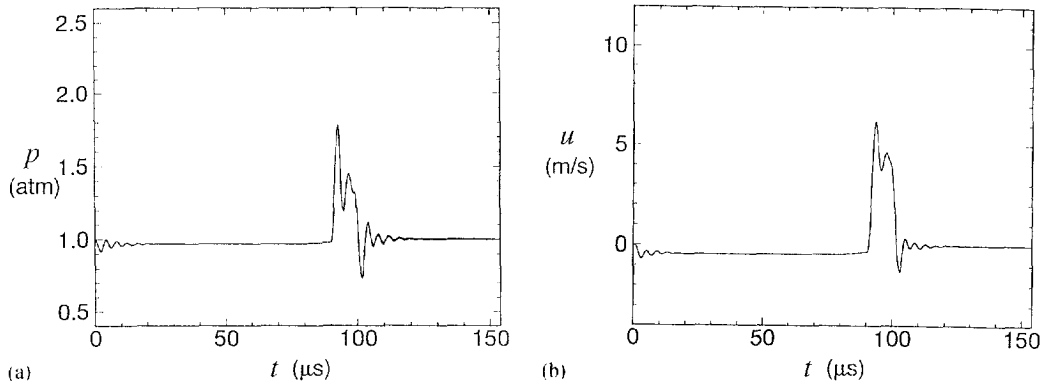

Fig. 11. (a) Numerical prediction of the pressure response history at T1 = 90 μs, T2 = 9 μs, T3 = 55 μs, and E = 25 V. (b) Numerical prediction of the velocity response history at T1 = 90 μs, T2 = 9 μs, T3 = 55 μs, and E = 25 V.

Table 1
Comparison of the measured and predicted ejected ink droplet weights for T1 = 90 μs, T3 = 55 μs, and E = 25 V at various T2 values

T2 value	Experimental droplet weight (ng)	Predicted droplet weight (ng)	error (%)
5	45.3	48.7	7.7
7	46.7	48.5	3.9
9	46.3	48.4	4.6
12	39.9	48.4	21.4
15	33.3	48.3	45

operating voltages is close to a constant value of 1.34 and is slighter lower than the voltage ratio of 1.67. A maximum ink droplet weight occurs at the same discharge time of 7 μs for both operating voltages. This is because the smaller pressure rise and the longer discharge time for a greater value of T2 have the opposite effect on the ink ejection weight.

The numerical predictions of the pressure and velocity response histories using the presented analytical models are respectively shown in Fig. 11a and b. Note that the pressure shown in Fig. 11a is obtained at the node next to the nozzle exit. Over the entire discharge time, the maximum pressure at this location is 0.18 MPa which is close to the value (3 bar = 0.30 MPa) reported by the European Patent Application [11]. At the nozzle inlet for the piezoelectric printhead with T1 = 90 μs, T2 = 9 μs, T3 = 55 μs, and E = 25 V, the maximum pressure predicted is 0.32 MPa which is much smaller than a typical value of 11 MPa in a thermal bubble printhead [3].

Table 1 lists the measured and predicted ejected ink droplet weights for T1 = 90 μs, T3 = 55 μs, and E = 25 V at various T2 values. The predicted weight is evaluated by integrating the transient velocity response over one whole period of the electrical pulse, as shown in Fig. 11b. The agreement

is quite good between experimental and numerical results with a maximum difference of 7.7% at T2 less than 9 μs. As the discharging time T2 increases, the exit velocity becomes lower and the total discharge time becomes larger. Thus, the weight integration is approach constant, this is because we neglected the surface tension at the nozzle exit. It is expected to have smaller measured values than predicted values because some ink is drawn back into the nozzle through surface tension after the breakup of the ejected droplet. In this study, the surface tension of ink was not modeled.

5. Conclusions

A characteristic method is used to solve the one-dimensional wave equation for the flow channel of a piezoelectric printhead to obtain the pressure response in the flow channel and the ejected ink velocity. The cross-sectional area in this flow channel is not fixed. In addition, an inexpensive optical system was set up to measure the ink ejection length and the weight of ejected ink droplet weight. Based on the numerical and experimental results, the following conclusions can be drawn.

1. A good agreement can be found between the predicted and measured weight of ejected ink droplets. However, the predicted values are always slightly higher than the measured ones for T1 = 90 μs, T3 = 55 μs, and $E = 25$ V.
2. No significant effect for both charging and resting time intervals on the ejected ink length has been found.
3. The ejected ink droplet length linearly increases with the operating voltage but decreases with the discharging time for fixed T1 and T3 values.
4. Higher operating voltage results in a larger ejected ink droplet for the operating voltage tested in the present study. However, there exits an optimal discharging time interval to obtain the largest ejected ink droplet if E, T1, and T3 are fixed. In the present test piezoelectrical printhead, the optimal time interval T2 is 7 μs for T1 = 90 μs and T3 = 55 μs. Thus, there are two ways to obtain smaller ejected ink droplets: by lowering the operating voltage, or by varying the discharge time T2 from the optimal value if the printhead requires a higher DPI (dot per inch) value.
5. In future studies, the surface tension of the ink and the shape of the ink ejected out of the nozzle should be considered in order to obtain more accurate predicted results. Meanwhile, we are still making efforts on the simulation of the ejected ink droplet by utilizing the obtained results as conditions. Also, the formation of satellite droplets should be studied.

Acknowlegdements

Financial support by the Dialer and Business Electronics cooperation under the contract number of 85-5-012 is deeply appreciated. The progress of this study could not be achieved without the help of engineers from the research and product development division of Dialer and Business Electronics cooperation.

References

[1] Whel WR. Ink-jet-printing: the present state of the art. Compeuro '89-3rd Annual European Computer Conf., Hamburg, West Ger., 8–12 May 1989;2/46–52.
[2] Mills RN. Ink jet printing: past, present and future. IS & T's 10th Int. Cong. on Advances in Non-Impact Printing Technologies, 1994;410–14.
[3] Ping-Hei Chen, Wen-Cheng Chen, Chang S-H. Bubble growth and ink ejection process of a thermal ink jet printhead. Int. J. Mech. Sci. 1997;39:683–95.
[4] Beasley JD. Model for fluid ejection and refill in an impulse drive jet. Photographic Sci Eng 1977;21:78–82.
[5] Bogy DE, Talke FE. Experimental and theoretical study of wave propagation phenomena in drop-on-demand ink jet devices. IBM J. Res. Dev. 1984;28:314–21.
[6] Shield TW, Bogy DB, Talke FE. Drop formation by DOD ink-jet nozzle: a comparison of experiment and numerical simulation. IBM J. Res. Dev. 1987;31:96–110.
[7] Fromm JE. Numerical calculation of the fluid dynamics of drop-on-demand jets. IBM J Res Dev 1984;28:323–33.
[8] Berchtold A. Simulation of a drop-on-demand print head with planar piezo-electric transducer. Compeuro '89-3rd Annual European Computer Conf, Hamburg, West Ger., 8–12 May 1989;2/53–5.
[9] Kline SJ, McClintock FA. Describing uncertainties in single-sample experiments. Mech. Eng. 1953;75:3–8.
[10] Hosono S, Abe T, Yonekubo S, Usui M, Yoshida M. Ink jet type recording head driving circuit. US Patent No. 5426454, 1995.
[11] Diahl Hermann O Th, Dr et al. Ink jet recording head. EP Patent No. 0573055A2, 1993.